IEEE Access
Multidisciplinary | Rapid Review | Open Access Journal

Date of publication xxxx 00, 0000, date of current version xxxx 00, 0000.

Digital Object Identifier 10.1109/ACCESS.2017.Doi Number

Deployable Hook Retrieval System for UAV Rescue and Delivery

Van Sy Nguyen[1,2], Jinwon Jung[1], Sanghoon Jung[1], Seonggun Joe[3], and Byungkyu Kim[2, 4]

[1]Korea Aerospace University, Department of Aerospace and Mechanical Engineering, Gyeonggi-do, 10540, Korea
[2]Korea Aerospace University, Department of Smart Drone Convergence, Gyeonggi-do, 10540, Korea
[3]The BioRobotics Institute, Scuola Superiore Sant'Anna, Pontedera, 56025, Italy
[4]Korea Aerospace University, School of Aerospace and Mechanical Engineering, Gyeonggi-do, 10540, Korea

Corresponding author: Byungkyu Kim (e-mail: bkim@kau.ac.kr).

This work was supported by 2018 Korea Aerospace University faculty research grant (grant number: 201801306) and the BK21 FOUR program through the National Research Foundation of Korea (NRF) funded by the Korean government (grant number: 5199990714521).

ABSTRACT The rapid development of unmanned aerial vehicles (UAVs) has helped expand their practical use to many industrial applications. However, UAVs sometimes suffer from a flight time limitation and/or a loss in communication. Such undesired malfunctions can endanger public safety and incur economic losses. This paper presents a new class of UAV that can retrieve a disabled or malfunctioned UAV from the ground. We developed a deployable hook retrieval system (DHRS) which integrates three principal mechanisms (*i.e.*, deployment, slider-linkage-release, and hook release). Each mechanism plays a role in deploying and retrieving multiple hooks while using a simple control strategy. Through a Finite Element Method simulation, the hook was topologically optimized in order to achieve a high strength while reducing weight. The deployed multiple hooks allow the device to capture the target regardless of its orientation. Due to these design strategies, object recognition using a computer vision was simply demonstrated by exploiting ORB and FLANN algorithms. Through an experimental study, we discussed the target range, success rate, and the practical uses that the DHRS could achieve. The results show that the proposed designs were versatile and consistently successful in capturing the targets while addressing constraints such as power consumption, computational load, and lack of prior knowledge or information about the target.

INDEX TERMS Unmanned aerial vehicles, Manipulators, UAV with retrieval system.

I. INTRODUCTION

Unmanned Aerial Vehicles (UAVs) have become an emerging technology due to their potential to be used in a wide range of new applications. Rapid industrial developments have created a new model for UAV use, which includes rapid logistics [1], food delivery [2], medical support [3], and surveillance service [4]. Notably, miniatured sensors and actuators have allowed them to perform various tasks that require high-resolution imaging and fast data processing; *e.g.*, 3D mapping [5], wildfire surveillance using IR cameras [6], and radiation surveys using Compton camera [7]. New UAV technology also enables other advanced industrial applications by facilitating interaction between humans and various environments [8], [9] (*i.e.*, construction, agriculture, air traffic management, disaster management, and telecommunication). As a result, the UAV market has grown rapidly, and it is anticipated that economic growth in industries exploiting UAVs will increase significantly [10].

From a public safety point of view, however, commercialized UAV use could create several problems [11] (*i.e.*, privacy and personal data protection, damage to physical objects, injuries to people on the ground, and potential risk to other airspace users). Hence, a number of countries have established regulations, including UAV registration and flight permits. Despite such governmental efforts, accidents due to the malfunction of UAVs are unavoidable. Such malfunctions occur by either a loss of communication or an airborne collision [12], [13]. For these reasons, the Federal Aviation Administration (FAA) in the USA implemented the unmanned aircraft system (UAS) sightings report to monitor UAVs' accidents through public records [14].

Similarly, many countries have also implemented an investigation database and reporting system [15], [16]. From an economic point of view, on the other hand, UAVs that can perform challenging missions (*i.e.*, an inspection of transmission towers or bridges [17], exploration in hazardous

This article has been accepted for publication in a future issue of this journal, but has not been fully edited. Content may change prior to final publication. Citation information: DOI 10.1109/ACCESS.2021.3080979, IEEE Access

terrain, or searching for victims in disasters [18], [19], etc.) are quite expensive due to the specialized embedded equipment they carry. Accordingly, retrieving and/or rescuing these UAVs could provide an opportunity to reduce maintenance expenses. In light of these preliminary facts, a subset system that embeds a rescue module, capable of towing, rescuing, and delivering, enables UAVs to ensure public safety and reduce costs.

To develop a subset system, it's necessary to develop a design that carefully addresses the specific constraints of UAV systems (*i.e.*, dimensions, power consumption, scalability, etc.) In terms of scalability, UAV size and battery capacity show a nonlinear relationship. To date, UAV flight time is largely dependent on further developments in battery power to weight ratios (*i.e.*, dramatic improvement in both battery capacity and reducing weight). A design strategy for the subset system should allow the device to be both lightweight and compact while ensuring high energy efficiency. UAV power consumption depends on the number of actuators and their efficiency, which can be appropriately addressed by either embedding high-efficiency actuators or by minimizing the number of actuators.

From a mechanical point of view, the aerial manipulator must embed a versatile mechanism that can dexterously perform a range of gripping and manipulation. In general, a conventional gripper follows a specific sequence (*i.e.*, approaching the target, gripping and manipulation, and releasing) and needs a grasping strategy that incorporates proprioception to perform multidimensional motions [20]. However, the grasping strategy requires prior knowledge of the target, which requires a complex control system and a high computational load. For example, proprioceptive sensors using vision system have shown promising potential [21], [22]; allowing the robots to perform multifunctional manipulation tasks. However, this method has its disadvantages- it has excessive computational complexity and/or the algorithm cannot be simplified. Recently, the algorithm has been further refined by means of reinforcement learning or artificial intelligence (AI) [23]-[25]. However, it is still a challenge to embed such an advanced system in UAVs, because the environmental conditions (*i.e.*, wind, rapid maneuvering, etc.) are quite unpredictable. Indeed, these conditions could cause the vehicle to follow unpredictable trajectories (*i.e.*, divergence or non-convergence to the desired course) and automatic control systems can follow undesired trajectories (*i.e.*, drift). Among these deviations, a ground effect occurs when the UAVs approach the ground because the reflected flows from the ground react with the UAV. Hence, it leads to an unstable attitude control.

In light of comprehensive findings on design strategies, rescue/delivery using an embedded subsystem should be performed when the UAV is sufficiently high above the ground to avoid any adverse ground effects. Furthermore, any grasping strategy should be simple and reliable, with an intuitive control system that reduces the algorithm complexity and its computational load. From mechanical point of view, the mechanism should be lightweight and compact, feature low power consumption by using a single actuator, and allow the system to operate at a sufficient distance above the ground.

This paper presents a deployable hook retrieval system (DHRS) that embeds a deployable capturing module with multiple cable-hooks which engage the target UAV. The design also incorporates a single, motor-driven deployment/release mechanism, which minimizes the power consumption while extending the available flight time. The cable-hook system was designed to reduce the computational load that the proprioceptive and/or exteroceptive sensor-based grasping strategy would require. Indeed, this advantage allows the DHRS to achieve versatile and dexterous grasping and manipulation, even though the orientation of the target is unpredictable and/or incomputable. Through a Finite Element Method (FEM) simulation, the design of the hook was topologically optimized in terms of strength, weight, and feasibility. In addition, recognition of the target UAVs was achieved by means of vision, which integrates with the proposed DHRS. To demonstrate the feasibility of the DHRS, we fabricated it and carried out indoor and outdoor experiments.

II. METHOD

A. CONCEPTUAL DESIGN

The main objective of this study is to implement a novel mechanism driven by a single motor, and to employ a cable, which allows the rescuing UAV to operate at a sufficient altitude to avoid any ground effect, as shown in Fig. 1.
Furthermore, if any UAV malfunctions occur, its orientation is unpredictable, and so the DHRS offers versatility with high deformability and adaptability. This section introduces rigorous design parameters to configure the mechanism adequately and describes a solution that addresses the issues. As shown in Fig. 2., the proposed DHRS consists of three mechanisms: the deploying mechanism, the slider-linkage-releasing mechanism, and the hook-releasing mechanism. These mechanisms are kinematically connected together and driven by a single motor.

The deploying mechanism consists of a motor, shaft, winch, holder, knob, and compression spring. Two holders clamp the knob and are fixed by the geared teeth of the winch. The position of the slider connected with the knob is also fixed by a compressed spring. Once the self-locking motor connected to the winch is triggered, the holders release the knob and slider, and the compression spring pushes the slide and displaces it along the guide tube. This mechanical process allows the linkages to uniformly deploy at the same speed, while enabling the DHRS to deploy linkages and wind the cables with a single motor.

This article has been accepted for publication in a future issue of this journal, but has not been fully edited. Content may change prior to final publication. Citation information: DOI 10.1109/ACCESS.2021.3080979, IEEE Access

The slider-linkage-releasing mechanism consists of a slider, linkages, multiple cables, and the assembly consisting of the guide frame, guide key, door key, and door. The guide key which interfaces with each linkage slot helps control the linkage angle at its deployed state. Once the slider reaches the end of the guide frame, the door key is then pressed, and the door is opened. Here, the main cables stored at the inside of the guide tube are passively released downwards due to gravity. According to the angle of the linkage, each hook can have a designated direction and initial velocity when it is released. Since the main cables are passively released, the hooks follow a parabolic motion without interference from the main cables.

The hook-releasing mechanism consists of a cable, spring, nut, and mobile bar. The mobile bar sustains the hook at the end of the linkage. Once the linkages are deployed, the mobile bar is guided along the central axis of the DHRS, and then the sustained hooks descend. The nut limits the displacement range of the mobile bar, and the spring compresses the mobile bar until the DHRS is deployed.

B. WORKING PRINCIPLE

This section describes the working process of DHRS at each phase. Once the DHRS is initiated by means of the geared motor, each phase can passively actuate without explicit control, as shown in Fig. 3.

The initial phase (A): The DHRS is placed under the parent UAV. The employed motor has a worm gearbox, which has a high torque and prevents the mechanism from operating in reverse. The self-locked gearbox allows the winch to fix its initial position, which enables the holders to clamp the knobs.

Releasing the holders/deploying the linkages (B): Once the parent UAV hovers above the target, the geared motor is then triggered by an operator. The winch unlocks the holder-knob-slider connection, and the compressed spring passively expands. The slider moves longitudinally due to the restoring force of spring, and the linkages are simultaneously deployed.

Descending hooks and main cable (C): The linkages are passively deployed, and each mobile bar moves along the central axis. Here, once the sliders reach and depress the key, the door opens, and the main cable stored in the guide tube is then released. Hence, the main cable and the hooks sustained at the linkages are released and descend, following a parabolic motion towards the disabled UAV.

Capturing the target (D): By winding the main cable with the motor, the descended hooks engage and attach to the malfunctioned UAV. As the main cable is further engaged, the DHRS then tows the target.

C. NUMERICAL STUDY USING FINITE ELEMENTS METHODS (FEM)

The primary objective of the simulation study is to obtain an optimized design for the hook and to investigate the feasibility of the proposed DHRS. In former cases, the hook needed a rigorous design, ensuring both adequate adaptability with respect to the target and adequate strength to support the imposed weight. Typically, the Ramshorn hook has been used for cranes that lift heavy loads [26]. Due to this, many industrial applications have widely used the hook [27]. To properly employ such a design with DHRS, the mechanical characteristics of the hook (*i.e.*, stress versus strain, stress concentration, strain energy, cyclic fatigue, design life, and safety factor) should be investigated to avoid failures due to imperfections or geometric irregularities. Notably, any stress concentration due to a given imposed weight should be solved. Also, the mechanical stability should be enhanced to accommodate fatigue.

The simulation was realized by using commercial FEM tools ANSYS 19.2 (ANSYS inc., Canonsburg, PA, USA), and we employed a static structural analysis. To allow for clear and straightforward analysis, we defined a basic hook configuration with a volume of 10,786 mm^3, as shown in Fig. 4. The inner radius at the highest stress point (r_1), the outer radius of the hook (r_2), the outline radius of the hook (r_3), and the angle of the hook tip (α) are identified as design parameters. The hook length (l), height (h), width (w), and thickness of the tip (t) are 25.5 mm, 17.5 mm, 9 mm, and 6 mm, respectively. A force of 40 N is applied at the inner surface of the hook, which would accommodate the payload of the parent UAV and the weight of DHRS. We defined each Type of hook, from Type 1 to 4, by topologically transforming the hook configuration. As will be described later, the hook was fabricated using 3D printing technology, and the material used was PLA (Poly Lactic Acid). The material properties are summarized [28] in Table 1.

To investigate a reliability of the optimal hook design, the fatigue analysis for each hook configuration was carried out under a zero-based loading condition (Stress ratio R=1). In this testing environment, any thermal or vibrational effects were disregarded. A safety factor against fracture strongly depends on the imposed load and/or deformation. Fatigue stress and/or residual stress could remain in the material structure. Accordingly, if the stress is concentrated on a weak part of the structure, mechanical failure could possibly occur, and the design life is reduced. For these reasons, the stress versus the "number of cycles to failure" (S-N curves) and the endurance limits associated with high-cycle fatigue (HCF) were examined [29]. The nodes of the interface were constrained to where the main cable mounts at the surface, and the imposed force was limited to an inner surface of the hook. The default minimum size of the mesh element was identified as 0.0458 mm. The generated meshes and the nodes were 38,809 and 63,604, respectively.

D. KINEMATIC MODEL OF THE DHRS

Once the mechanism is deployed from the DHRS, the impulsive force (f_{ip}) could be created by the impact (Q_{ip}). In

This article has been accepted for publication in a future issue of this journal, but has not been fully edited. Content may change prior to final publication. Citation information: DOI 10.1109/ACCESS.2021.3080979, IEEE Access

general, the impact has a linear relationship with the impulsive force and the time (*dt*) that the collision lasts, as follows:

$$Q_{ip} = \int_0^t f_{ip} \cdot dt \tag{1}$$

The impulsive force is proportional to the restoring force (F_k=$f_{iu}x$) created by the compressed spring due to the quasi-static equilibrium. The time (*dt*) is also a dependent parameter for the spring constant. To better analyze the kinematics of the presented DHRS, we neglected all possible friction forces and considered the variation of the potential energy from the initial state (U_1) to the ejected state (U_2). Then, according to the law of the conservation of energy, the potential energy of the compressed spring is equal to the kinematic energy of the deployable mechanism, which can be expressed by:

$$U_{1\to 2} = \frac{1}{2} f_{iu} x^2 - \frac{1}{2} M v^2 = 0 \tag{2}$$

where f_{iu} and x indicate a spring constant and a deformation of the compression spring, and M and v indicate the total mass of the deployable mechanism and its velocity when it ejects from the initial state.

As shown in Fig. 5., once the linkage is displaced along the path of the arc (l=$\pi L \cdot \theta$), each hook undergoes a centrifugal force (F_l), and can be expressed as follows:

$$F_l = mL \cdot w^2 \tag{3}$$

$$w = \pi \sqrt{\frac{f_{iu} x}{mL}} \tag{4}$$

where w, m and L denote the angular velocity, the weight of hook and the length of the linkage, respectively. When the hooks are deployed from the linkage, the velocity ($\vec{V}_{P_0}$) can be written as:

$$\overrightarrow{V_{P_0}} = \pi \sqrt{\frac{f_{iu} x \cdot L}{mN}} \cdot \breve{n} - \boldsymbol{g} \cdot t \tag{5}$$

$$\breve{n} = \begin{bmatrix} cos\phi cos\theta \\ sin\phi cos\theta \\ sin\theta \end{bmatrix}$$

$$\boldsymbol{g} = [0 \quad 0 \quad -g]^T \tag{6}$$

where $\breve{n}$ and $\boldsymbol{g}$ are the norm vector of the velocity and the gravity vector, respectively. g and t are the acceleration due to gravity and time, respectively. Here, since the trajectory of the hooks follows the parabolic motion, the vector $\overrightarrow{r_{P_0}}$ is represented by:

$$\overrightarrow{r_{P_0}} = \int_0^T \overrightarrow{V_{P_0}} \cdot dt \tag{7}$$

From the expression of $\overrightarrow{r_{P_0}}$, the required time (T) to reach at P_1 can be expressed:

$$T = \frac{r_{P_0,x}}{|\overrightarrow{V_{P_0}}| \cdot cos\phi cos\theta} \tag{8}$$

Which can be substituted into the expression of $r_{P_0,z}$ and the target range (R) can also be expressed:

$$r_{P_0,z} = \frac{r_{P_0,x} \cdot tan\theta}{cos\phi} - \frac{1}{2} g \left(\frac{r_{P_0,x}^2}{cos^2\phi}\right)\left(\frac{1+tan^2\theta}{\vec{V}_{P_0}^2}\right) \tag{9}$$

$$R = \left|\overrightarrow{V_{P_0}}\right| \cdot T \cdot cos\theta \tag{10}$$

From (5) to (10), we identified crucial parameters which determine the target range and the impulsive force correlated with the spring constant and the deployed angle (θ) of the linkage. In general, the axial stiffness of compression spring is a function of its dimensions, as follows:

$$f_{iu} = \frac{G}{8} \cdot \frac{d^4}{D^3 \cdot n} \tag{11}$$

where G is the shear modulus, and d, D, and n are the diameter of the wire, the mean diameter of spring, and the number of active coils, respectively.

E. OBJECT RECOGNITION

A real time-based computer vision interface was built in order to recognize and localize the targeted UAV. Among the local feature-based algorithms [30]-[32], the ORB was employed due to its fast image processing time [32], [33]. In preliminary studies on classes of local feature-based algorithms, ORB with low feature-points detection (less than 1,000) was the most efficient and ensured promising characteristics (*i.e.*, computational efficiency, the efficiency of feature-matching per feature-point, speed efficiency, etc.), compared to other algorithms (*i.e.*, BRISK, SURF, SIFT, AKZE, and KAZE) [34]. Wherein the FLANN algorithm matches descriptors quickly [35]. Therefore, the combination of ORB and FLANN is helpful in implementing the vision-aided system; ensuring a simple and efficient process which is able to adapt to inflexible external factors. With this in mind, we employed the ORB algorithm as a descriptor and FLANN as a matcher to build a real time-based computer vision interface for the DHRS. The local feature-based algorithm converts images from RGB to grayscale in order to simplify the information [36]. Moreover, employing a field of view (FoV) provides a promising opportunity to reduce the computational delay up to 50 % [37]. The region of interest (RoI) is identified to align both the centers of the target and the parent UAV. Here, the computed orientation of the parent UAV includes inherent errors, while it does not exceed a target range that the DHRS could have, as will be detailed next section. Therefore, the embedded vision-aided proprioceptive sensing solution could provide a promising opportunity by recognizing the object without exteroceptive sensors or any grasping strategy utilizing prior knowledge or information. To achieve an efficient and simple computer vision system, we limited the number of feature-points (less than 500), which were determined through indoor tests. For early demonstration, we employed a main processor (NVIDIA®, Jetson Nano, US), providing a high clock speed (4 core ARM at 1.43 GHz), memory (4 GB and 64 bit) and

This article has been accepted for publication in a future issue of this journal, but has not been fully edited. Content may change prior to final publication. Citation information: DOI 10.1109/ACCESS.2021.3080979, IEEE Access

storage (16 GB) as well as very low power consumption (up to 25 W).

III. RESULTS

A. OPTIMIZATION OF THE HOOK DESIGN

As shown in Fig. 6., the simulation results show that Type 1 undergoes a stress concentration at the edge of the hook, and it could lead to a fracture. To relieve the concentrated stress, a curvature having a radius (r) was employed. The central structure undergoes an extension stress due to the imposed load. Thus, we changed its cross-section from square to cylindrical. This transformation distributes the stress along the whole structure. The imposed load strongly influences the inner layer and the central cylinder, rather than the outer layer. It indicates that Type 2 could be a beneficial design to relieve the concentrated stress along the structure (reduce the maximum stress to 35.1%), compared to Type 1. Type 3 is designed to reduce the weight of the structure (12.8% reduction). The optimal hook (Type 4), with the best mechanical performance and the lightest weight, was obtained by combining the best features of Type 2 and 3.

As a result, Type 4 showed enhanced structural stability and evenly distributed stress along the inner surface and central cylinder of the hook. From a structural safety point of view, it indicates that the structure is reliable, without any indications of mechanical failure for the imposed deformation or weight. Particularly, through Types 1 to 4, the stress is uniformly distributed. Indeed, as a result of fatigue analysis, the endurance limit of Type 4 does not exceed its inherent material strength, which implies that it can withstand nearly unlimited cycles (up to 10^6) with a safety factor of 2.44 and an imposed force of 40 N. Detailed values of design parameters and simulation results for each Type are summarized in Table 2.

Based on the simulation results, Type 4 was identified as the best hook, ensuring optimal dimensions with the lightest weight, while avoiding fracture and fatigue failure. We fabricated the Type 4 hook using a 3D printer (GIANTBOT, G-005, 380 x 380 x 380 mm^3, South Korea) and demonstrated the feasibility of the DHRS.

B. VALIDATION OF TARGET RANGE (R) OF THE DHRS

The target range (R) corresponds to the diameter of the circle obtained from the deployment of the hooks. In principle, the diameter can be approximated by means of (3) and (10). To evaluate the performances of DHRS, experimental setups were built by using a circular grid with quadrants. We performed six trials to confirm the repeatability and reliability of the target range (See the supplementary video S1), and the DHRS placed at 2 m in z-axis, as depicted in Fig. 7(a) and (b). By exploiting vision analysis, global coordinates and kinematic trajectories for each hook were obtained, as shown in Fig. 7(c). The trajectory of the hooks follows a parabolic motion. Once the hooks are separated from the linkages, it rapidly forms a target range and then falls free towards the ground.

The employed compression spring exhibited an axial stiffness of 0.138 N/mm, with an error of 31 %, compared to the theoretical value (0.105 N/mm). In Fig. 7(d), the x-axis velocity when the hooks were separated from the linkages was measured to 1,365.1 mm/s, with an error of 13.3% compared to theoretical velocity (1,574.44 mm/s). Such difference between the measurement and the theoretical value was mainly obtained by means of energy dissipation due to the friction between the mechanical components and/or the viscosity of air. Indeed, the dissipated energy was 0.54 J, which accounts for 78.4% of the potential energy that the compression spring can produce (0.69 J). As shown in Fig. 7(e), all trials showed that the hooks were properly distributed at each quadrant. The target range (R) was approximated by using a direct least-square circle fitting [38]. As a result, the target range of 453.29 mm was obtained with an error of 49.1%, compared to the theoretical value (890.636 mm).

C. SUCCESS RATE VERSUS ECCENTRIC TARGET

The parent UAV could possibly fail to capture and manipulate the targeted UAV due to any misalignments between them. Such undesired misalignments have been addressed by means of vision-aided control and navigation system [39]-[41], yet it is still a challenge to precisely control the UAV without imposing an excessive computational load on the system [42]. Moreover, undesired trajectories (*i.e.*, drift, coupling effect) could be significant due to various environmental conditions. For these reasons, UAVs that embed conventional grippers need a grasping strategy with a complex control algorithm. Hence, given the possibility that errors could occur, we investigated the success rate. In this investigation, the error is measured according to the eccentric distance from the desired target, which forms a rational basis to determine when the DHRS should be operated. The experimental setups were built according to eccentric distances, ranging from 0 to 500 mm, with steps of 200 mm, as shown in Fig. 8(a) to (d). The eccentric distance was measured using the vision-aided system (see Fig. 8(e)). Here, the white and yellow dots refer to the center of the DHRS and the center of the targeted UAV, respectively. Also, each circle colored in green and red corresponds to the reference scales of 400 mm and 200 mm, respectively. The blue-colored square indicates a range of keypoint clusters. Fig. 8(f) shows RoI captured from a real time video; the colored small circles and lines correspond to the feature-points and valid matches, respectively. As a result, up to 95% accuracy was measured, and 246 features were detected.

The diameter of the targeted UAV was 550 mm (DJI®, F550, China), and we performed five trials for each condition. To evaluate the capturing performance, a statistical analysis was carried out by using categorical and discrete variables (*i.e.*,

This article has been accepted for publication in a future issue of this journal, but has not been fully edited. Content may change prior to final publication. Citation information: DOI 10.1109/ACCESS.2021.3080979, IEEE Access

the number of the snagged hooks, the tilted angle, and stability of target, etc.). We employed a Kruskal-Wallis ANOVA analysis to determine the correlation between the number of snagged hooks and the eccentric distance. The number of snagged hooks was significantly reduced at the eccentric distance of 200 mm (p-value: 0.0046), and the number continued dropping as the eccentric distance approached 500 mm (p-value: 0.0067). As a result of interpolation, a linear response was obtained (R^2=0.92), as shown in Fig. 8(g). Secondly, we employed a tertile, dividing the ordered distribution into three categorical sets, with respect to the tilted angle ranging from 0 to 90º (*i.e.*, Low, Medium, and High). Then, we assigned the stability of the target from High to Low with respect to the tilted angle. As shown in Fig. 8(h), the fewer the engaged hooks, the more unstable the captured target became (p-value: 0.08); and resulted in a high tilted angle (60~90º), which indicates a high failure probability. In spite of the ability of the DHRS to pick up the target with one engaged hook, we observed the target was dropped during the manipulation. In light of these findings, an eccentric distance of 200 mm still allows the parent UAV to successfully capture a targeted UAV with a diameter of 550 mm. In particular, the proposed DHRS can achieve its desired performance and ensure a high success rate of 77.87% (the area of eccentric distance (A_e) / the area of target rage (A_D)), even if the embedded vision recognition system had any errors.

D. TOWARDS A NEW CLASS OF VERSATILE GRIPPER

The presented DHRS was validated through an outdoor test. Furthermore, we demonstrated its practical uses as a new class of versatile gripper. In the outdoor test, the parent UAV carried DHRS and maneuvered at an altitude of 2 m, allowing the DHRS to operate. A commercial drone (DJI, Spreading Wings S900, china), having a max thrust force of 82 N and default weight of 3.3 kg, was employed. In terms of power consumption, a DC motor (Motorbank, WGM32, South Korea) integrated into DHRS has a gear ratio of 1:123 and produces a high torque of 1.8 kgf·cm at 48 rpm (rev/min). The motor power is approximately 2.28 W (input voltage of 12 V and current of 190 mA). Since the operating time of DHRS from hook deployment to lifting the target was less than 50 seconds, the energy consumption of the DC motor (114 J) was insignificant compared to the battery capacity of the parent UAV. On the other hand, target UAV payloads (ranging from 1 to 4 kg) and the weight of DHRS (750 g) strongly influence flight time. According to the datasheet [43], we calculated that the parent UAV could have a flight time of up to 18 min at a total weight of 6.8 kg, with a resulting energy consumption of approximately 1,080 kJ. Therefore, it can be tentatively concluded that energy consumption is a factor of payload, and that a single-driven mechanism ensures high energy efficiency.

Meanwhile, the impulsive force and/or impact due to the deployment of DHRS were negligible since the parent UAV is capable of lifting a high payload. As shown in Fig. 9(a)., we observed that the trajectory of the UAV was stationary. Furthermore, we identified that an altitude of 2 meters ensures stability without undesired trajectories, and thus the DHRS picked up the target successfully and manipulated it (see the supplementary video S2). In addition to the purposes of towing, rescuing, and delivering the UAV, we demonstrated its potential to perform versatile gripping tasks for objects with different shapes or configurations. As shown in Fig. 9(b) and Table 3., various objects with different configurations and dimensions were used. As a result, if more than three hooks were engaged, all objects were successfully picked up.

IV. DISCUSSION AND CONCLUSION

This paper presents a novel mechanism capable of towing, rescuing, and delivering the malfunctioned UAV. The major contribution of this work is to introduce a rigorous design for a capturing mechanism that can conserve computing resources by reducing necessary grasping sequences (*i.e.*, pose estimation, grasp detection, and motion planning), and ensure a high success rate in capturing the target. The proposed DHRS consists of three principal mechanisms. By employing a cable, it can allow the hooks to deploy and retrieve the target without needing a complex control strategy. The hook was employed in order to ensure successive opportunities to capture the target, regardless of orientation or any errors that might occur due to environmental conditions or other external factors. The mechanical characteristics of the hook were investigated by means of numerical simulation, and an optimal configuration was obtained, which combined both high strength and minimal weight. The indoor experiments were carried out according to the eccentric distance. We evaluated the possible target range of the DHRS, and analyzed it using the derived kinematic model.

The proposed system is also scalable and can achieve a longer target range. The size of the parent UAV and the DHRS can be proportionally scaled up to accommodate larger or heavier targets. Increasing DHRS target range or distance can be achieved by enhancing the axial stiffness of the deployment spring. The kinematic model identified that the velocity ($\vec{V}_{P_0}$) was proportional to the square root of axial stiffness of the compression spring and inverse of mass, respectively. Accordingly, if the axial stiffness is adequately increased without an increase of mass (*e.g.*, increasing wire diameter, using heavier materials, etc.) the DHRS's mechanical performances, including the target range, could be further improved.

As demonstrated by the indoor and outdoor experiments, DHRS endows UAVs with the ability to perform tasks in areas where a safe landing is impossible. Furthermore, DHRS ensured a high capture success rate of 77.87 %, within an eccentric distance of 200 mm. Due to this range of inaccuracy that the DHRS can accommodate, the computational load of the vision system can be reduced. Compared to traditional gripper mechanisms [44]-[46], the proposed DHRS also

proved more versatile, and we demonstrated its ability to successfully capture a wide range of irregularly shaped objects, regardless of the configuration or dimension of the target object. These findings will allow us to develop a straightforward grasping strategy for difficult objects to be sensed and grasped (*e.g.*, complex geometry, deformable objects).

However, the presented DHRS has several limitations that need to be overcome in future work. First, because releasing the rescued UAV is an essential task that the gripper should perform, it needs a mechanism that can release the target. One possible solution is to integrate a new mechanism into the DHRS which is capable of releasing the target. However, this modification should be carefully evaluated in terms of payload, available workspace, opening angle etc. Secondly, the types of objects that can be successfully gripped are limited to those which have physical features that allow the hook to snag the object. An adhesion technology could be used so that the hook more easily engages flat surfaces. It might be possible for the hooks to mechanically engage or snag the bottom edge of an object with flat surfaces after the object is first lifted by means of adhesion force. Thirdly, DHRS needs further refinements to its mechanical characteristics; such as payload capacity, actuation stiffness and/or density.

Although the presented DHRS needs further development and study, we hope the comprehensive results from this study lay the groundwork for an emerging technology; a new type of gripper system with its own unique advantages and applications.

REFERENCES

[1] J. G. Carlsson, and S. Song, "Coordinated logistics with a truck and a drone," *Management Science,* vol. 64, no. 9, pp. 4052-4069. 2018.

[2] J. Hwang, and J. Y. J. Choe, "Exploring perceived risk in building successful drone food delivery services," *International Journal of Contemporary Hospitality Management*. 2019.

[3] P. P. Ray, and K. Nguyen, "A Review on Blockchain for Medical Delivery Drones in 5G-IoT Era: Progress and Challenges," *2020 IEEE/CIC International Conference on Communications in China (ICCC Workshops)*, pp. 29-34. 2020.

[4] F. Nex, and F. Remondino, "UAV for 3D mapping applications: a review," *Applied geomatics,* vol. 6, no. 1, pp. 1-15. 2014.

[5] E. Guisado-Pintado, D. W. Jackson, and D. Rogers, "3D mapping efficacy of a drone and terrestrial laser scanner over a temperate beach-dune zone," *Geomorphology,* vol. 328, pp. 157-172. 2019.

[6] S. Samiappan, L. Hathcock, G. Turnage, C. McCraine, J. Pitchford, and R. Moorhead, "Remote sensing of wildfire using a small unmanned aerial system: post-fire mapping, vegetation recovery and damage analysis in Grand Bay, Mississippi/Alabama, USA," *Drones,* vol. 3, no. 2, pp. 43. 2019.

[7] S. Mochizuki, J. Kataoka, L. Tagawa, Y. Iwamoto, H. Okochi, N. Katsumi, S. Kinno, M. Arimoto, T. Maruhashi, and K. Fujieda, "First demonstration of aerial gamma-ray imaging using drone for prompt radiation survey in Fukushima," *Journal of Instrumentation,* vol. 12, no. 11, pp. P11014. 2017.

[8] A. Otto, N. Agatz, J. Campbell, B. Golden, and E. Pesch, "Optimization approaches for civil applications of unmanned aerial vehicles (UAVs) or aerial drones: A survey," *Networks,* vol. 72, no. 4, pp. 411-458. 2018.

[9] H. Yao, R. Qin, and X. Chen, "Unmanned aerial vehicle for remote sensing applications—A review," *Remote Sensing,* vol. 11, no. 12, pp. 1443. 2019.

[10] M. Mazur, A. Wisniewski, and J. McMillan, "PwC global report on the commercial applications of drone technology," *PricewaterhouseCoopers, tech. Rep.* 2016.

[11] C. Stöcker, R. Bennett, F. Nex, M. Gerke, and J. Zevenbergen, "Review of the current state of UAV regulations," *Remote sensing,* vol. 9, no. 5, pp. 459. 2017.

[12] M. J. Schuurman, B. Rattanagraikanakorn, C. Kassapoglou, and R. De Breuker, "Urban air mobility (UAM) vehicle design considerations to facilitate future accident investigation," *AIAA Aviation 2019 Forum*, p. 3628. 2019.

[13] Wang, J., Jiang, C., Han, Z., Ren, Y., Maunder, R. G., and Hanzo, L. "Taking drones to the next level: Cooperative distributed unmanned-aerial-vehicular networks for small and mini drones." *IEEE vehIcular technology magazine*, vol. 12, no. 3, pp. 73-82. 2017.

[14] R. J. Wallace, T. Haritos, and J. Robbins, "Building Evidence the Federal Aviation Administration's UAS Safety Strategy Needs Improvement," *International Journal of Aviation, Aeronautics, and Aerospace,* vol. 5, no. 1, pp. 10. 2018.

[15] N. Tsiamis, L. Efthymiou, and K. P. Tsagarakis, "A Comparative Analysis of the Legislation Evolution for Drone Use in OECD Countries," *Drones,* vol. 3, no. 4, pp. 75. 2019.

[16] G. Wild, K. Gavin, J. Murray, J. Silva, and G. Baxter, "A post-accident analysis of civil remotely-piloted aircraft system accidents and incidents," *Journal of Aerospace Technology and Management,* vol. 9, no. 2, pp. 157-168. 2017.

[17] S. Chen, D. F. Laefer, E. Mangina, S. I. Zolanvari, and J. Byrne, "UAV bridge inspection through evaluated 3D reconstructions," *Journal of Bridge Engineering,* vol. 24, no. 4, pp. 05019001. 2019.

[18] A. A. Ravankar, A. Ravankar, Y. Kobayashi, and T. Emaru, "Autonomous mapping and exploration with unmanned aerial vehicles using low cost sensors," *Multidisciplinary Digital Publishing Institute Proceedings,* vol. 4, no. 1, p. 44. 2018.

[19] M. Silvagni, A. Tonoli, E. Zenerino, and M. Chiaberge, "Multipurpose UAV for search and rescue operations in mountain avalanche events," *Geomatics, Natural Hazards and Risk,* vol. 8, no. 1, pp. 18-33. 2017.

[20] G. Du, K. Wang, S. Lian, and K. Zhao, "Vision-based robotic grasping from object localization, object pose estimation to grasp estimation for parallel grippers: a review," *Artificial Intelligence Review,* pp. 1-58. 2020.

[21] P. Werner, M. Hofer, C. Sferrazza, and R. D'Andrea, "Vision-Based Proprioceptive Sensing: Tip Position Estimation for a Soft Inflatable Bellow Actuator," *2020 IEEE/RSJ International Conference on Intelligent Robots and Systems (IROS)*, 2020.

[22] Y. She, S. Q. Liu, P. Yu, and E. Adelson, "Exoskeleton-covered soft finger with vision-based proprioception and tactile sensing." *2020 IEEE International Conference on Robotics and Automation (ICRA)*, pp. 10075-10081. 2020.

[23] B. Shih, D. Shah, J. Li, T. G. Thuruthel, Y.-L. Park, F. Iida, Z. Bao, R. Kramer-Bottiglio, and M. T. Tolley, "Electronic skins and machine learning for intelligent soft robots," *Science Robotics*, vol. 5, no. 41. 2020.

[24] A. Carrio, C. Sampedro, A. Rodriguez-Ramos, and P. Campoy, "A review of deep learning methods and applications for unmanned aerial vehicles," *Journal of Sensors*, vol. 2017. 2017.
[25] S. Caldera, A. Rassau, and D. Chai, "Review of deep learning methods in robotic grasp detection," *Multimodal Technologies and Interaction*, vol. 2, no. 3, pp. 57. 2018.
[26] A. Manee-ngam, P. Saisirirat, and P. Suwankan, "Hook design loading by the optimization method with weighted factors rating method," *Energy Procedia*, vol. 138, pp. 337-342. 2017.
[27] N. Khan, G. Bhushan, and P. Chandna, "Design and Stress Analysis of Ramshorn Hook with Different Cross Section using CAE Tools," *International Journal of Engineering Technology Science and Research*, pp. 1-8. 2017.
[28] S. Farah, D. G. Anderson, and R. Langer, "Physical and mechanical properties of PLA, and their functions in widespread applications—A comprehensive review," *Advanced drug delivery reviews*, vol. 107, pp. 367-392. 2016.
[29] G. Gomez-Gras, R. Jerez-Mesa, J. A. Travieso-Rodriguez, and J. Lluma-Fuentes, "Fatigue performance of fused filament fabrication PLA specimens," *Materials & Design*, vol. 140, pp. 278-285. 2018.
[30] D. G. Lowe, "Distinctive image features from scale-invariant keypoints," *International journal of computer vision*, vol. 60, no. 2, pp. 91-110. 2004.
[31] H. Bay, A. Ess, T. Tuytelaars, and L. Van Gool, "Speeded-up robust features (SURF)," *Computer vision and image understanding*, vol. 110, no. 3, pp. 346-359. 2008.
[32] E. Rublee, V. Rabaud, K. Konolige, and G. Bradski, "ORB: An efficient alternative to SIFT or SURF," *2011 International conference on computer vision*, pp. 2564-2571. 2011
[33] S.-Y. Guan, T.-M. Wang, C. Meng, and J.-C. Wang, "A review of point feature based medical image registration," *Chinese Journal of Mechanical Engineering*, vol. 31, no. 1, pp. 76. 2018.
[34] Tareen, Shaharyar Ahmed Khan, and Zahra Saleem. "A comparative analysis of sift, surf, kaze, akaze, orb, and brisk." *2018 International conference on computing, mathematics and engineering technologies (iCoMET)*. IEEE, pp. 1-10. 2018.
[35] Muja, Marius, and David G. Lowe. "Fast approximate nearest neighbors with automatic algorithm configuration." *International Conference on Computer Vision Theory and Application (VISSAPP)*, pp. 331–340. 2019.
[36] A. Güneş, H. Kalkan, and E. Durmuş, "Optimizing the color-to-grayscale conversion for image classification," *Signal, Image and Video Processing*, vol. 10, no. 5, pp. 853-860. 2016.
[37] A. Al-Kaff, F. García, D. Martín, A. De La Escalera, and J. M. Armingol, "Obstacle detection and avoidance system based on monocular camera and size expansion algorithm for UAVs," *Sensors*, vol. 17, no. 5, pp. 1061, May. 2017.
[38] V. Pratt, "Direct least-squares fitting of algebraic surfaces," *ACM SIGGRAPH computer graphics*, vol. 21, no. 4, pp. 145-152. 1987.
[39] M. Sanfourche, J. Delaune, G. Le Besnerais, H. De Plinval, J. Israel, P. Cornic, A. Treil, Y. Watanabe, and A. Plyer, "Perception for UAV: Vision-Based Navigation and Environment Modeling," *AerospaceLab*, pp. 1-19. 2012.
[40] C. Demonceaux, O. Morel, and D. Fofi, "Vision based uav attitude estimation: Progress and insights," *Journal of Intelligent & Robotic Systems*, vol. 65, no. 1-4, pp. 295-308. 2012.
[41] H.-M. Chuang, D. He, and A. Namiki, "Autonomous target tracking of UAV using high-speed visual feedback," *Applied Sciences*, vol. 9, no. 21, pp. 4552. 2019.
[42] A. J. Barry, H. Oleynikova, D. Honegger, M. Pollefeys, and R. Tedrake, "Fast onboard stereo vision for UAVs," *Vision-based Control and Navigation of Small Lightweight UAV Workshop, International Conference On Intelligent Robots and Systems (IROS)*, 2015.
[43] Spreading Wings S900 Specification, [online] Available: https://www.dji.com/it/spreading-wings-s900.
[44] J. Shintake, V. Cacucciolo, D. Floreano, and H. Shea, "Soft robotic grippers," *Advanced Materials*, vol. 30, no. 29, pp. 1707035. 2018.
[45] K. Tai, A.-R. El-Sayed, M. Shahriari, M. Biglarbegian, and S. Mahmud, "State of the art robotic grippers and applications," *Robotics*, vol. 5, no. 2, pp. 11. 2016.
[46] J. Hughes, U. Culha, F. Giardina, F. Guenther, A. Rosendo, and F. Iida, "Soft manipulators and grippers: a review," *Frontiers in Robotics and AI*, vol. 3, pp. 69. 2016.

This article has been accepted for publication in a future issue of this journal, but has not been fully edited. Content may change prior to final publication. Citation information: DOI 10.1109/ACCESS.2021.3080979, IEEE Access

FIGURES

FIGURE 1. Conceptual design of the deployable hook retrieval system (DHRS);

This article has been accepted for publication in a future issue of this journal, but has not been fully edited. Content may change prior to final publication. Citation information: DOI 10.1109/ACCESS.2021.3080979, IEEE Access

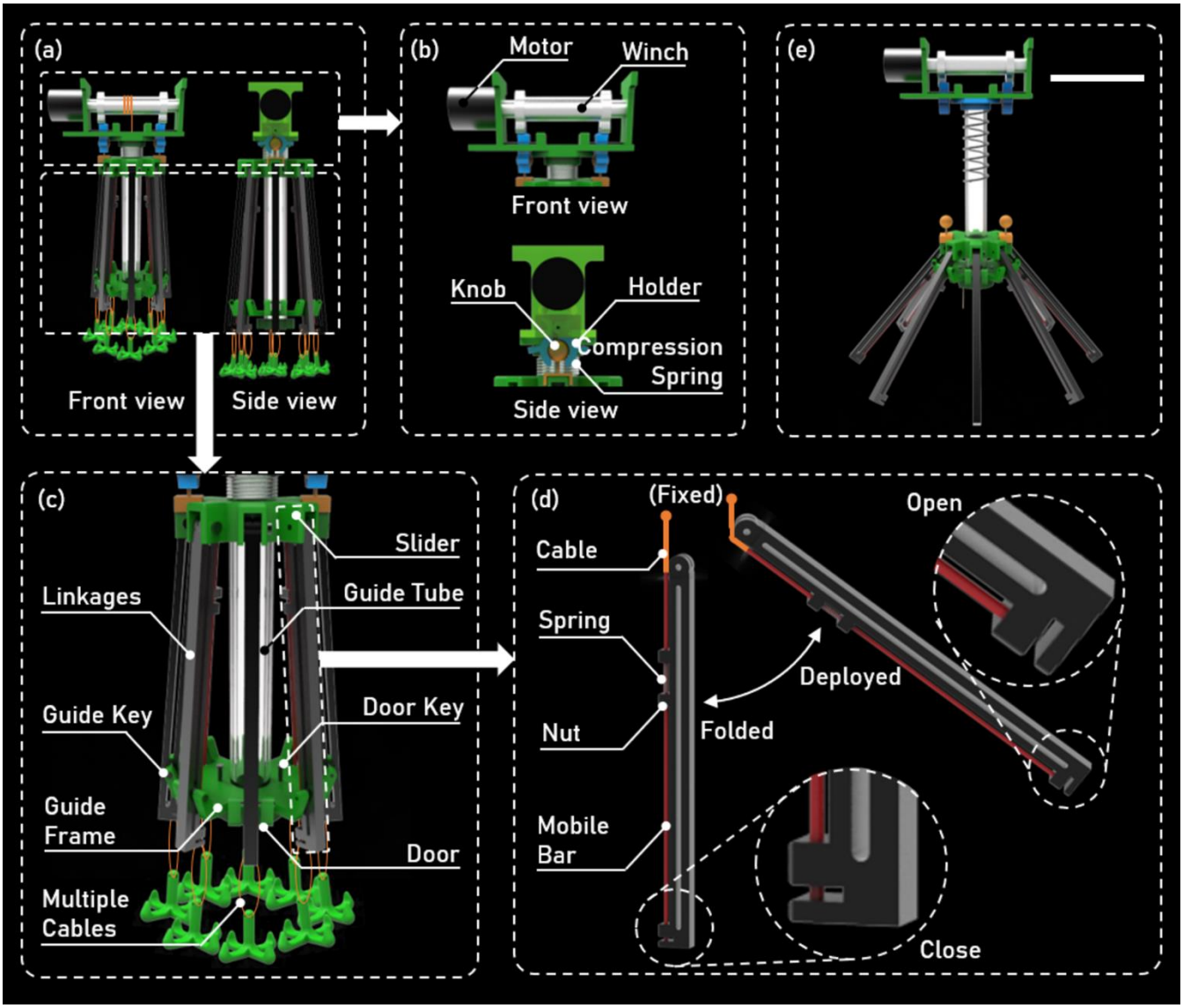

FIGURE 2. **Mechanical components of the deployable hook retrieval system (DHRS); (a) Front (left) and side (right) views at the folded state, (b) Deploying mechanism, (c) Slider-linkage-releasing mechanism, (d) Hook-releasing mechanism at the folded and deployed states, respectively, (e) DHRS at the deployed state (scale is 100 mm).**

This article has been accepted for publication in a future issue of this journal, but has not been fully edited. Content may change prior to final publication. Citation information: DOI 10.1109/ACCESS.2021.3080979, IEEE Access

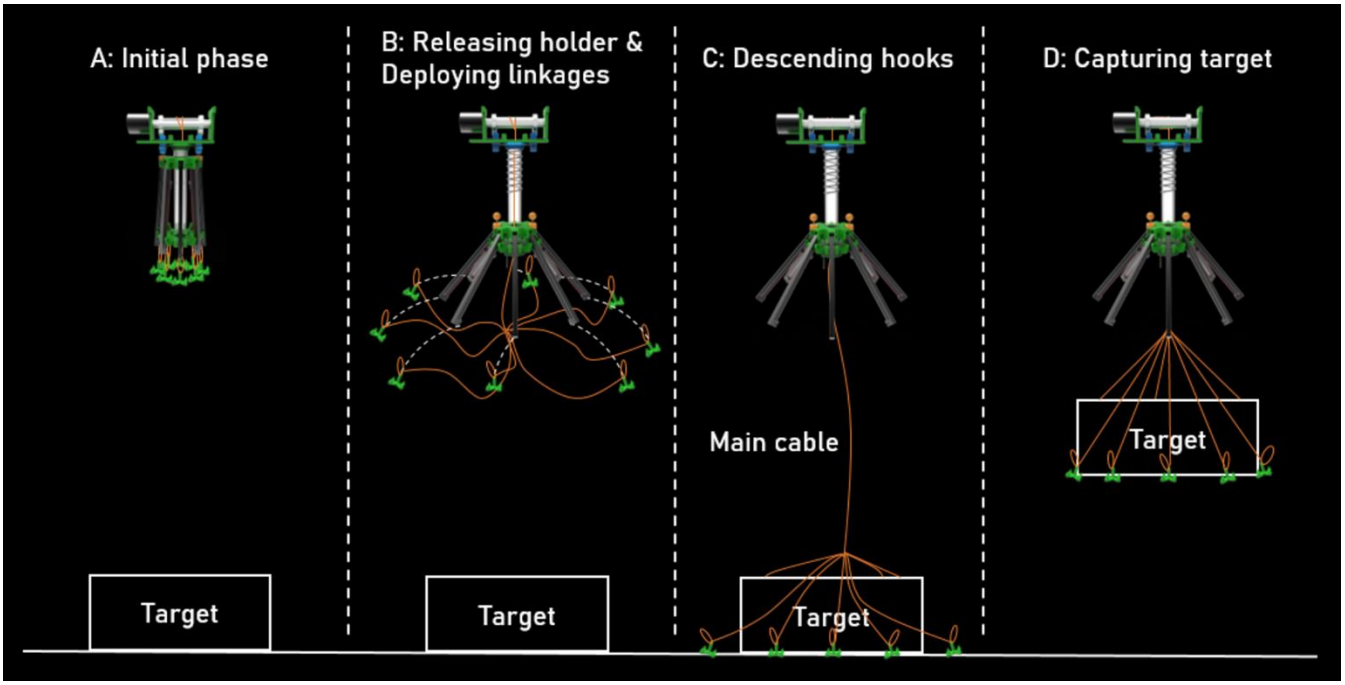

FIGURE 3. The working principle of the DHRS, showing each phase from the initial phase (A) to the capturing target (D).

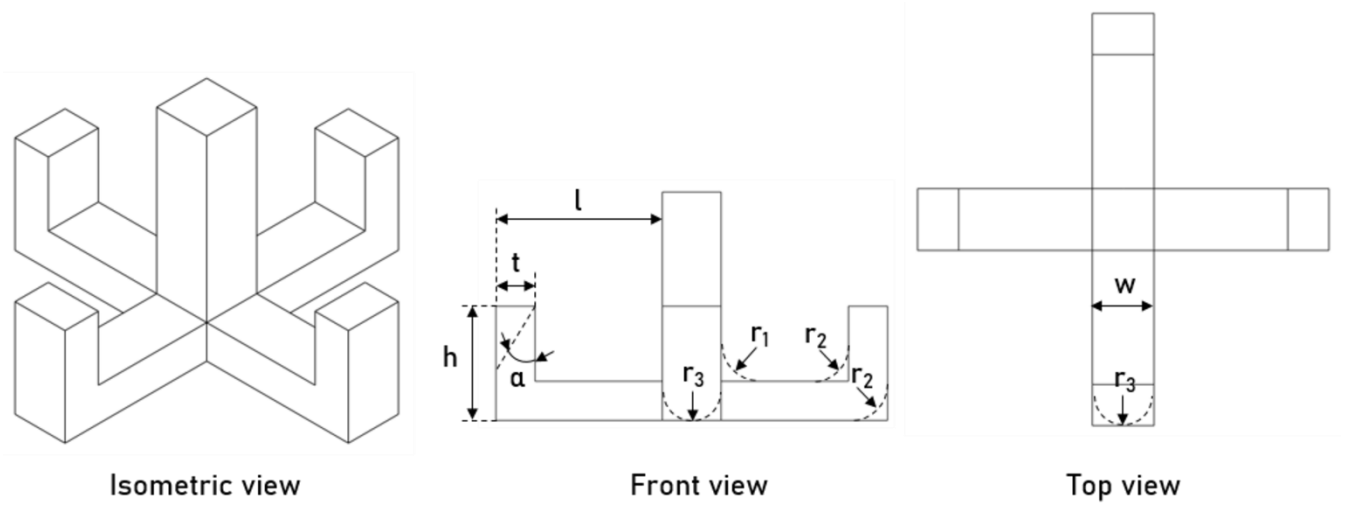

FIGURE 4. Topological transformation and design parameters of the hook.

This article has been accepted for publication in a future issue of this journal, but has not been fully edited. Content may change prior to final publication. Citation information: DOI 10.1109/ACCESS.2021.3080979, IEEE Access

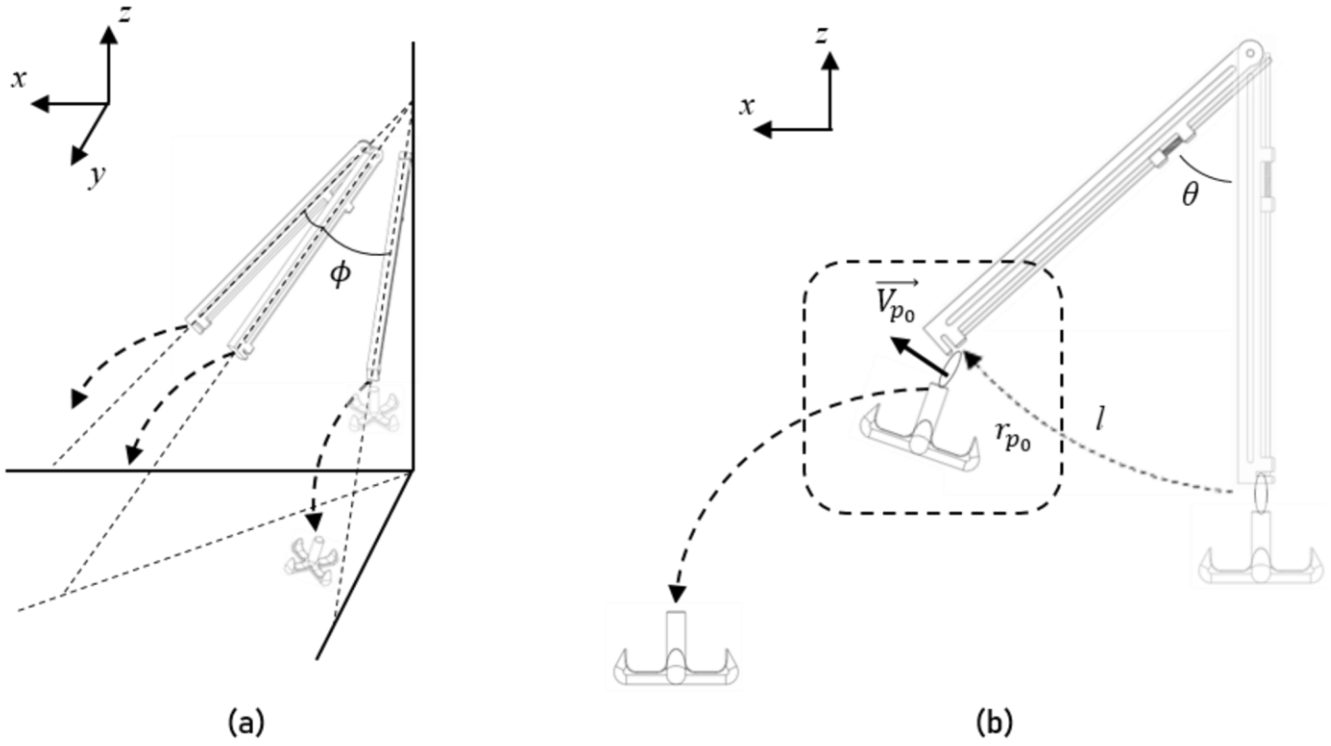

FIGURE 5. The kinematic model of DHRS; (a) Isometric view. (b) Side view.

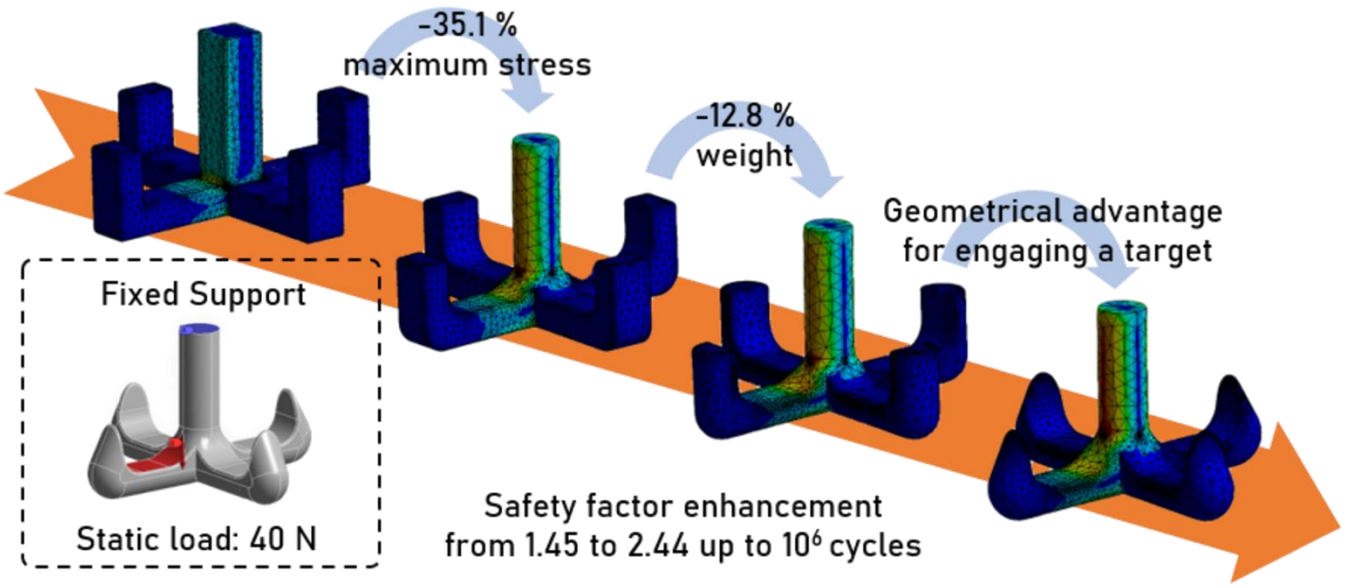

FIGURE 6. Simulation setup and demonstration of the topological transformation of the hook, responding to stress, weight reduction, and safety factor.

This article has been accepted for publication in a future issue of this journal, but has not been fully edited. Content may change prior to final publication. Citation information: DOI 10.1109/ACCESS.2021.3080979, IEEE Access

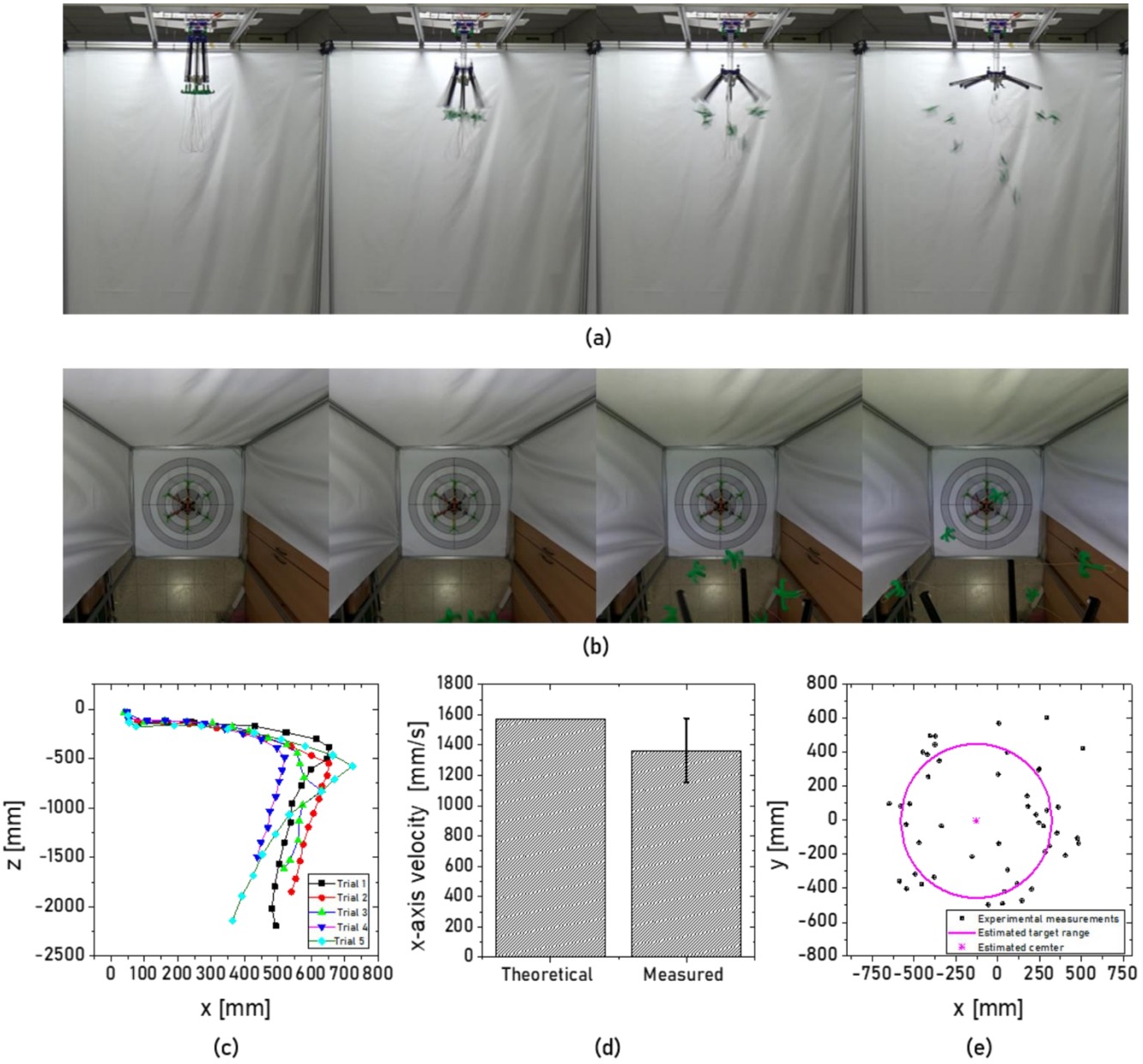

FIGURE 7. Experimental results; the fabricated DHRS deploys the linkages and releases the multiple hooks. Photographs of (a) Side view and (b) Top view were obtained by means of a high frame rate (0.018 sec interval). (c) Trajectories of the hooks at xz plane. (d) Theoretical (1,574.44 mm/s) and experimental x-axis velocity (1365.1 mm/s, std: 213.429) of the hook. (e) The estimated target range (Pink line) and center (Pink dot) with respect to the experimental measurements of the deployed hooks.

This article has been accepted for publication in a future issue of this journal, but has not been fully edited. Content may change prior to final publication. Citation information: DOI 10.1109/ACCESS.2021.3080979, IEEE Access

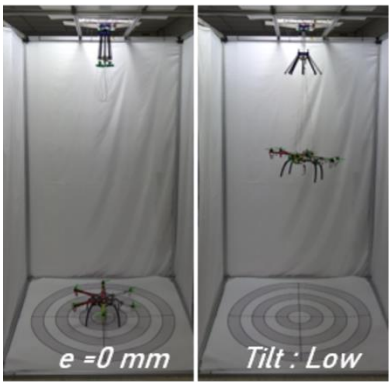

(a)

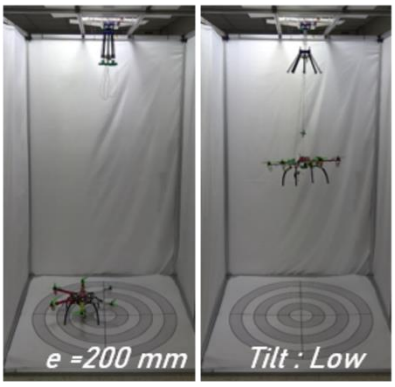

(b)

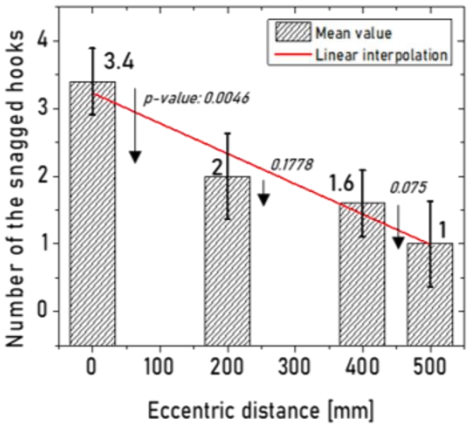

(g)

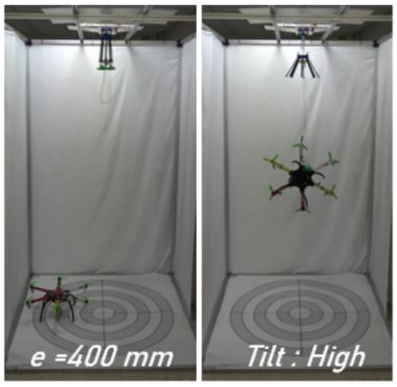

(c)

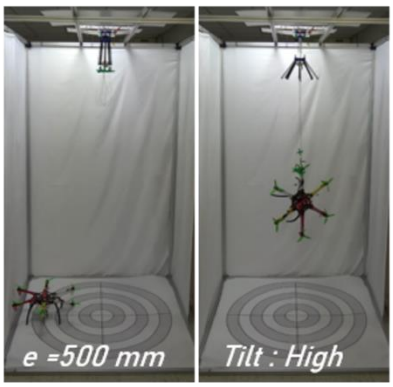

(d)

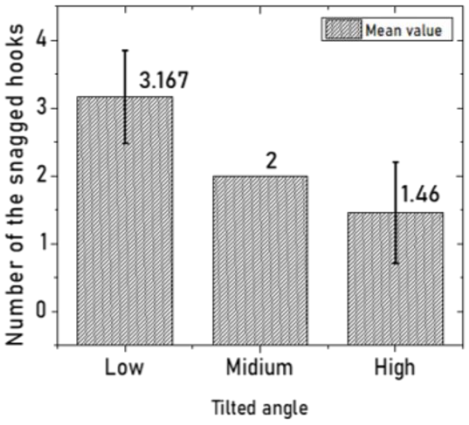

(h)

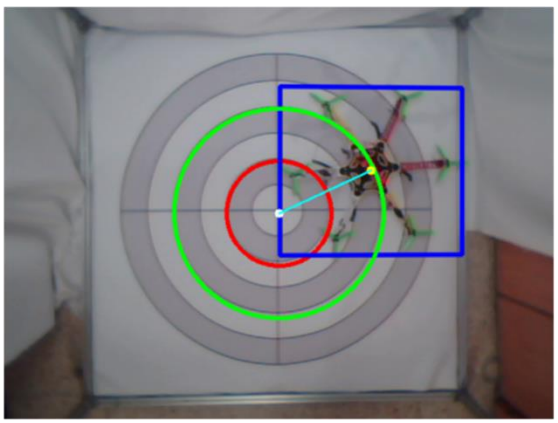

(e)

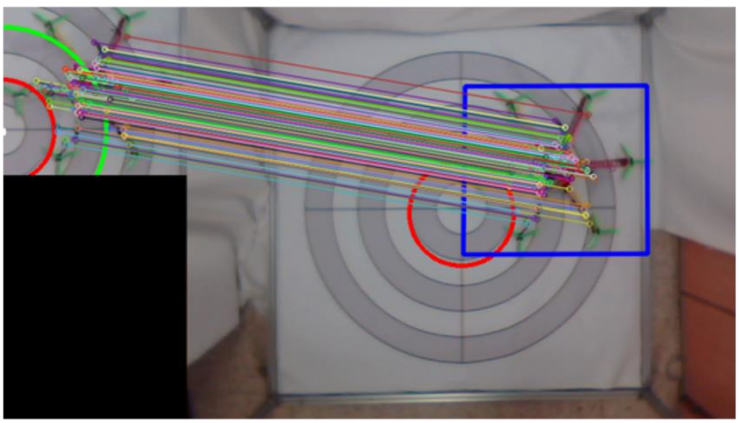

(f)

FIGURE 8. Photographs of the experimental studies showing the initial state (Left) and the captured target (Right) at the eccentric distances of (a) 0 mm, (b) 200 mm, (c) 400 mm and (d) 500 mm. (e) an eccentric distance obtained from the vision aided system (white dot: center of DHRS, yellow dot: center of the targeted UAV). (f) Region of Interest captured from a real time video (colored circles and lines indicate the feature-points and valid matches, respectively). (g) The relationship between the eccentric distances and the number of the snagged hooks (P-value 0.0067, Kruskal-Wallis ANOVA analysis). (h) The relationship between the tilted angle and the number of snagged hooks.

This article has been accepted for publication in a future issue of this journal, but has not been fully edited. Content may change prior to final publication. Citation information: DOI 10.1109/ACCESS.2021.3080979, IEEE Access

FIGURE 9. (a) The DHRS equipped with the parent UAV performed desired tasks (approaching the target, capture, pick-up, manipulation) at the outdoor experiment. (b) Versatile capturing capabilities with respect to unknown dimensions of the targets.

This article has been accepted for publication in a future issue of this journal, but has not been fully edited. Content may change prior to final publication. Citation information: DOI 10.1109/ACCESS.2021.3080979, IEEE Access

TABLES

TABLE 1. Material properties of PLA

Parameter	Value
Density	1.252 [g/cm3]
Young's Modulus	1280 [MPa]
Poisson's Ratio	0.36
Tensile Yield Strength	59 [MPa]
Tensile Ultimate Strength	73 [MPa]

TABLE 2. Design parameters and simulation results of hook optimization

	Design parameters				Simulation results		
	r_1 [mm]	r_2 [mm]	r_3 [mm]	α [degree]	Maximum Stress [MPa]	Weight [g]	Safety factor
Type 1	-	-	-	-	16.62	13.51	1.45
Type 2	4.5	4.5	-	-	10.79	13.13	2.23
Type 3	5	5	4.5	-	10.74	11.45	2.24
Type 4	5	5	4.5	30	9.89	10.38	2.44

*Length parameters are constant (t=6, w=9, l=25.5, h=17.5 [mm])

TABLE 3. Dimensions of unknown objects

Case	Height (mm)	Length (mm)	Width (mm)
I	220	340	420
II	510	510	510
III	350	520	400
IV	240	260	600